Eurographics Workshop on Natural Phenomena (2009)
E. Galin and J. Schneider (Editors)

Procedural Modeling of Leather Texture with Structural Elements

Kaisei Sakurai [1] , Kazunori Miyata [2] , Naoki Kawai [1] and Kazuo Matsufuji [1]

[1] Dai Nippon Printing Co. Ltd., Japan
[2] Japan Advanced Institute of Science and Technology, Japan

Abstract

This paper proposes a simple generation method for realistic leather texture. Leather surface consists of five structural elements, which are cristae, sulci, wrinkles, pockets and pores, which characterize the visual impression of the leather texture. We classified structural elements by observing real leather surface. To represent the elements, the method extracts features of real textures in order to generate an outline of each element. Then the method computes each element is three-dimensional shapes by a function which defines a continuous surface. Our method generates detailed leather texture, and is easy to handle, with simple procedures and intuitive parameters.

Categories and Subject Descriptors (according to ACM CCS): Computer Graphics [I.3.7]: Three-Dimensional Graphics and Realism - Color, shading, shadowing, and texture—

1. Introduction

Leather is one of the most popular materials for the surfaces of daily products such as chairs, bags, shoes, and wallets. Leather is tanned skin of animals such as cattle, horses, pigs, goats, sheep, reptiles etc., and most (estimated 90 %) commercial leather products are made from cattle leather.
The leather texture is also important in computer graphics for improving reality of rendered surfaces of such products. Height field for bump mapping can often be obtained by means of measuring a surface [CGS06, HEG01] or procedural texture generation. Though the measuring techniques obtain precise surface details, it is difficult to modify a region of captured texture by hand. Procedural texture generation methods generate various patterns depending on user-specified parameters, however an independent method is required for each object, and the results often lack reality or detailed geometry. This paper describes a procedural leather texture generation which is focused on the structural elements of cattle leather, which is sufficient for improving the appearance of generated textures.

2. Related Works

Many procedural texturing techniques have been developed to represent color or geometry of surfaces, such as stone [Miy90, DEJ*99], biotic patterns [Tur91, WK91] etc. [PPWE02, PH89, Wor96].
There are several related procedural methods for leather and skin. Ishii et al. applied Bezier curve to modify a Voronoi diagram to generate human skin texture [IYYT93]. McCartney et al. applied Voronoi diagram to generate a leather texture [MHZ94]. Wu et al. proposed generation methods for wrinkles [WKT96, WKT97, WKMT99]. Their methods define sulci as Delaunay edges, and they generate wrinkles along sulci.
Some procedural leather texture generation methods considered cell-cell interaction by means of particle simulation for representation of surface detail. Itoh et al. found that arrangement and crista of cristae show anisotropy [IMS03], that is to say they are directionally dependent. They give anisotropic energy function to control particles as cell motion on skin surface to generate anisotropic distribution of points that represent an arrangement of cristae. They also placed pieces of arbitrary shapes onto generated points, and constructed a Pseudo-Voronoi diagram based on placed pieces. Miyata et al. considered microscopic structure of a leather surface. They proposed a method for representing small bumps on a crista by means of blobs [MSI*06]. Sakurai et al. proposed a method for generating sulci flow on leather surface [SMKM07]. They assumed that cracks on leather form sulci and proposed a method for crack

simulation. The method generates meso-structure of leather textures, however it still lacks some noticeable structures.
Texture synthesis [HB95, SP98, DB97, EL99, WL00, ZWM98, ZZV*03] has been proposed to reconstruct a new texture image in any size without visual repetition from a sample as input. The textures obtained by these methods however depend on the pattern (arrangements, structures and etc.) of the input, and the methods are unsuitable to generate various patterns.
In this paper, we propose a simple generation method for various realistic textures of cattle leathers, considering obvious structures.

3. Modeling Leather Surface

3.1. Definition of Structural Elements

Fig. 1 shows several typical examples of cattle leather measured by a 3D scanner. Although each texture looks different from others, they also seem to consist of common structural elements. The structural elements can be classified by several noticeable elements.
We classify elements into five types listed below, and assume that any cattle leather textures can be formed with aggregates of the five elements.

1) Crista
2) Sulcus
3) Wrinkle
4) Pocket
5) Pore

The most noticeable structure of the leather texture is a reticulated pattern which consists of furrows. We define a mesh encircled with looped furrows as a Crista, as shown in Fig. 2(a). Some furrows look like independent line elements segmented by nodes, and others look like series of connected segments. We define an independent one as a Sulcus and a series as a Wrinkle, as shown in Fig. 2(b). Wrinkles run along mostly in the same direction, in the case of Fig 1(a), from top to bottom. Sulci form a depression at their shared node and we define it as a Pocket, as shown in Fig. 2(a). A surface of crista is not smooth, there are many tiny holes scattered over it, and we define them as Pores, as shown in Fig. 2(c).

3.2. Details of Observation

Fig. 3 shows an enlarged image of a pocket. A sulcus penetrates the next pocket and cracks the next crista slightly. Fig. 4(a) shows an enlarged image from Fig. 1(a), and Fig. 4(b) shows a manual binarization of Fig. 4(a). In Fig. 4(b), wrinkles appear as solid lines while sulci appear as broken lines. This observation indicates that most areas of wrinkles are deeper than a threshold height while most areas of sulci are shallower.
We also assume that both cracks on cristae and wrinkles are formed by crumpling on skin surface. That is, crumpling adds stress on the leather surface, and the stress elongates sulci thereby cracking cristae. In the case of strong stress, sulci crack and cross over cristae, and thus the sulci connect with each other. Also, the stress widens the connected sulci.

The arrangement of cristae looks anisotropic, and we prove it as follows. We are not interested in individual shape of each crista, so we analyze anisotropy of cristae by means of power spectral density applied on a height field, as shown in Fig. 5. The high frequencies indicate microscopic bumps on the surface, and arrangement of cristae appears at low to middle range frequencies as a dense ring in frequency domain. The ring appears unclear as shown in 5(b), and this shows that the cristae tend to form horizontally flat on the

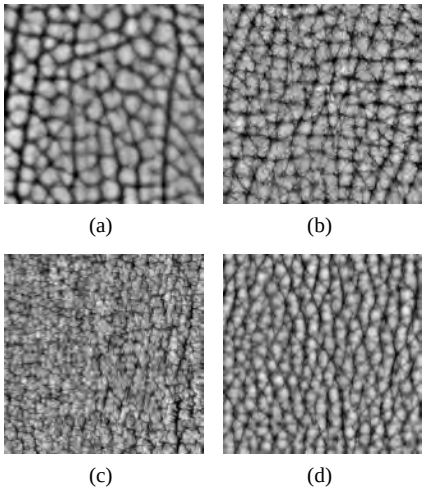

Figure 1: *Height fields of several types of leather texture. (the darker, the deeper).*

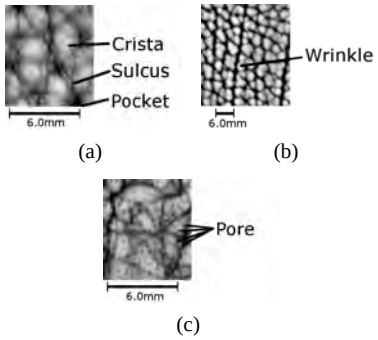

Figure 2: *Structural elements. Images show noticeable structural elements. (a) shows cristae, sulci and pockets. (b) shows wrinkles. (c) shows pores.*

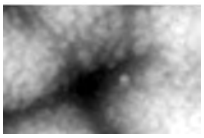

Figure 3: *A crack on the enlarged image of Fig. 1 (a). A sulcus penetrates a pocket and cracks the next crista from left to right.*

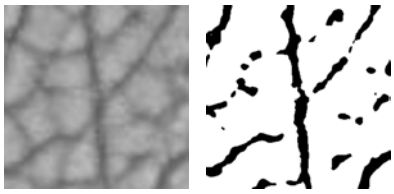

(a) (b)

Figure 4: *Binarized image. (a) is an enlarged image of sulci. (b) is a binarized image of (a).*

leather surface shown in Fig. 5(a). We next observe cross-sections of each structural element, and the border where two different elements adjoin. Fig. 6(a) - (c) show cross-sections of some combinations of typical elements that reconstructed from measured height field Fig. 1, and borders between two elements look unclear.

By observing these cross-sections, we can distinguish one element from others by its elevation and gradient of its slope. First of all, both sulci and wrinkles show sharper peaks than cristae do. Also, only cristae show convex section. Though the cross-section of pockets looks similar to cristae at first sight, it also approximates the section of wrinkles by scaling linearly as shown in Fig. 7. These observations suggest that the profiles of all elements except for cristae can be approximated by the same function. We can also distinguish wrinkles from sulci by their wider and deeper valley profile. Pockets are much wider than wrinkles, although their depth is similar to winkles. On the other hand, profiles of all elements look almost symmetry.

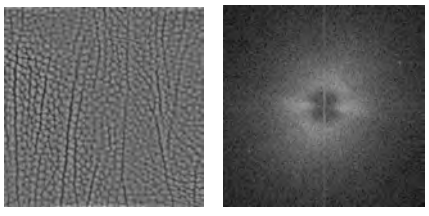

(a) (b)

Figure 5: *Two-sided power spectral density of leather. (a) a height field. (b) power spectral density of (a)*

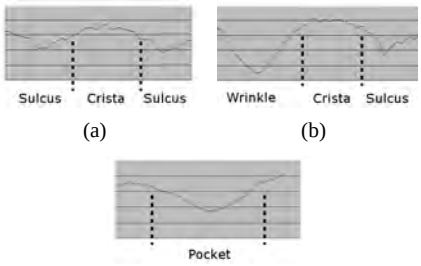

(a) (b) (c)

Figure 6: *Cross sections of typical elements. Broken lines indicate assumed borders. (a) a crista between two sulci. (b) a crista between a wrinkle and a sulcus. (c) a pocket.*

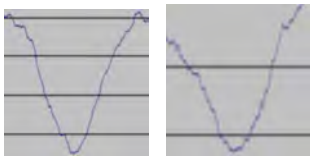

(a) (b)

Figure 7: *Cross section of (a) a wrinkle, and (b) a scaled pocket*

4. Generating Leather Surface

In this chapter, we propose a procedure for generating leather texture as a height field that includes all of the structural elements described in the previous chapter. The procedure first generates lines and points that represent skeletons of structural elements over the entire region. Then the procedure constructs the entire height field based on the distance from neighboring skeletons.

4.1. Constructing Skeletons

The procedure for generating skeletons consists of the following four steps. In the first step, the outlines of cristae, sulci and pockets are generated as a Voronoi diagram with anisotropically distributed sites, for representing anisotropy appearing in cristae, as observed in the previous chapter. The Voronoi regions, the Voronoi edges and the Voronoi vertices define skeletons of cristae, sulci and pockets, respectively. The end points of sulci are moved inside the next cristae for representing cracks in the second step. Then the third step makes skeletons of wrinkles by combining two or more sulci. The procedure places points for micro pores inside each crista in the last step.

4.1.1. Anisotropic Point Distribution for Voronoi Diagram

The procedure first generates a Voronoi diagram with sites which have been distributed at anisotropic intervals. For anisotropic distribution of Voronoi sites, we apply a modified Poisson-disk distribution. Conventional methods for Poisson-disk distribution such as Dart throwing, Lloyd's relaxation and tile based methods arrange points isotropically using an isotropic exclusive region. In contrast to those methods, our modified method refers to an anisotropic exclusive region, that is ellipse, which results in anisotropically distributed points. Here, the method adopts Dart throwing as the simplest implementation to alter and define the exclusive region. The procedure iterates the following sequence until the distributed points fill the entire region.

1. Select a point randomly
2. Place a new site on the point if the point is located outside of the exclusive region
3. Add a new exclusive region, at the center of which is located the new site

After the iterations have been completed, a Voronoi diagram is generated from distributed sites.

4.1.2. Cracks on Cristae

The obtained Voronoi edges represent skeletons for sulci. Cracks on cristae can be assumed to be extended sulci as we have observed. For simulating this formation process, each sulcus should be elongated depending on direction and amplitude of given stress, and new end points $\boldsymbol{p}_{new}$ of the Voronoi edge are calculated from a corresponding Voronoi edge $\overline{\boldsymbol{p}_1\boldsymbol{p}_2}$ by Eq. 1.

$$\boldsymbol{p}_{new} = \boldsymbol{p} + L(\boldsymbol{p} - (\boldsymbol{p}_1 + \boldsymbol{p}_2)/2) \tag{1}$$

By substituting both $\boldsymbol{p}_1$ and $\boldsymbol{p}_2$ for $\boldsymbol{p}$, two new end points appear on both sides of the original Voronoi edge, and a crack can be represented as a new line segment connecting the new point with the original Voronoi vertex,
where the length coefficient L is given by Eq. 2.

$$L = l \mid \boldsymbol{v}_{edge} \cdot \boldsymbol{b} \mid \tag{2}$$

l is an adjustment parameter for L, $\boldsymbol{v}_{edge}$ is a unit direction vector of the original edge as given by Eq. 3, and $\boldsymbol{b}$ represents the direction and amplitude of cracking caused by external stress.

$$\boldsymbol{v}_{edge} = nor(\boldsymbol{p}_1 - \boldsymbol{p}_2) \tag{3}$$

where $nor(\boldsymbol{v})$ is normalization function for $\boldsymbol{v}$.

4.1.3. Forming Wrinkles

Wrinkles seem to be relatively straight and we assume they can be formed as a series of connected sulci. Our method selects the first Voronoi edge randomly, and connects appropriate line segments toward given direction $\boldsymbol{b}$ one by one until the entire length reaches pre-defined length b_l.
Fig. 8 illustrates the operation that connects a new line segment with the forming wrinkle at the end point $\boldsymbol{p}_a$, and Fig. 9 shows the algorithm. The red line represents the last line segment of a forming wrinkle, and the next two line segments $\overline{\boldsymbol{p}_a\boldsymbol{p}_b}$ and $\overline{\boldsymbol{p}_a\boldsymbol{p}_c}$ are candidates for the next component of the wrinkle. To keep the wrinkle almost straight, the method connects a new segment within the crossing angle under given threshold b_a.
The method first compares the angles between $\boldsymbol{b}$ and $\overline{\boldsymbol{p}_a\boldsymbol{p}_b}$ and between $\boldsymbol{b}$ and $\overline{\boldsymbol{p}_a\boldsymbol{p}_c}$, and selects the segment which has a sharper angle as the final candidate.
If the angle b_{pabn}, between $\boldsymbol{b}$ and the candidate segment, is less than the threshold b_a, the method connects the candidate segment to the forming wrinkle as the last line segment. Or, the method generates a new vertex $\boldsymbol{p}_n$ at the intersection of the ray from $\boldsymbol{p}_a$ toward the vector $\boldsymbol{b}$ and the opposite side of Voronoi polygon, and the new line segment $\overline{\boldsymbol{p}_a\boldsymbol{p}_n}$ is connected to the wrinkle as the last line segment.

Figure 8: *Forming a Wrinkle. The red line segment belongs to a wrinkle. The green line segment becomes the next part of the wrinkle if the measure of the angle b_{pabn} is less than the threshold b_a, or the red broken line segment becomes the next part.*

$tmp1 \leftarrow$ angle between $\overline{\boldsymbol{p}_b\boldsymbol{p}_a}$ and $\boldsymbol{b}$
$tmp2 \leftarrow$ angle between $\overline{\boldsymbol{p}_c\boldsymbol{p}_a}$ and $\boldsymbol{b}$
if $tmp1 < tmp2$
  then $b_{pabn} \leftarrow tmp1, p \leftarrow p_b$
  else $b_{pabn} \leftarrow tmp2, p \leftarrow p_c$
if $b_{pabn} < b_a$
  then output $(\overline{p_a p})$
output $(\overline{p_a p_n})$

Figure 9: *Algorithm for connecting a new wrinkle line segment.*

4.1.4. Placing Pores

Pores are scattered on cristae. The procedure places a given number of points, which represent the positions of pores randomly over the entire region.

4.2. Calculating the Entire Height Field

Our method applies a functional modeling technique, Radial Basis Function (RBF), to represent the symmetrical three dimensional shapes of each of the five structural elements. RBF represents the function of one variable, for instance a distance, and is a simple and sufficient method for representing curved surfaces.
Our method defines gentle slopes which appear on cristae with Eq. 4, and steep slopes which appear on sulci, wrinkles, pockets and pores with Eq. 5.

$$H_c(d) = h_c(1 - \phi_c(d)) \tag{4}$$

$$H_v(d) = -h_v(\phi_v(d)) \tag{5}$$

Sulci, wrinkles, pockets and pores have independent $H_v(d)$ with unique parameters, and each $H_v(d)$ takes the distance between arbitrary position $\boldsymbol{x}(\forall \boldsymbol{x} \in \mathbb{R}^2)$ and the nearest target element. Regarding crista, a distance d is given as distance from the site of the polygon.
H_c and H_v represent the height at $\boldsymbol{x}$, and h_c and h_v are the height coefficients of the functions. RBF ϕ_c and ϕ_v are defined as in Eq. 6 and 7 with width w_c and w_v.

$$\phi_c(d) = \begin{cases} (d/w_c)^n, & (d < w_c) \\ 1, & otherwise \end{cases} \tag{6}$$

$$\phi_v(d) = \begin{cases} (1 - d/w_v)^4(4d/w_v + 1), & (d < w_v) \\ 0, & otherwise \end{cases} \tag{7}$$

RBF ϕ_c is given by compact supported n-th polynomial function, and RBF ϕ_v is given by Wendland RBF [Wen95].
The width w_c of Eq. 6 is defined by the distance between the site and the surrounding Voronoi edge, and other parameters can be defined arbitrarily.
The height at $\boldsymbol{x}$ is calculated independently as a crista, a sulcus, a wrinkle, a pocket and a pore, then the five heights are summed and this results in the final height at the position. Our method obtains the entire leather texture by calculating height at all sampling points.

5. Results and Discussion

Fig. 10 shows results of Poisson-disk distribution. The arrangement of sites distributed using an elliptical exclusive region shows anisotropy, while a circular exclusive region generates isotropic distribution.
Fig. 11 shows a Voronoi diagram calculated from two groups of sites, which have anisotropy in orthogonal direction from each other. The generated Voronoi regions show anisotropy horizontally and vertically, as well as the arrangement of original sites.
Fig. 12 shows the effects of some characteristic parameters. We generated each texture using parameters listed in Table 1. As we can see here, parameters h_s, w_s, l, and b_n represent the depth of sulci, the width of sulci, encroaching and number of wrinkles, respectively; these intuitive parameters enable easy control of texture and style.
Fig. 13 shows a generated height field from the simulation shown in Fig. 1(a). Fig. 14 shows a cross-section of the generated leather surface. The features observed in Fig. 6 are well reproduced in microscopic geometry. Fig. 15 shows power spectral density of the generated leather texture and proves our method generates anisotropic leather.
Fig. 16 shows examples of rendering with generated texture under different parameters for sulcus depth, sulcus width, and number of wrinkles.
This implementation requires about a minute to calculate 500 x 500 pixel leather textures with Intel Pentium 4 3.5 GHz processor and 1 GB RAM. Most procedures require under a second, but the shaping procedure needs most of the processing time for grid subdivision to search the nearest diagram.
The proposed method reproduces leather texture including all the observed elements, and the generated images are more realistic than previous methods. In addition, the proposed procedures are simple and not time-consuming, so that the method makes trial and error with changing parameters more practical.

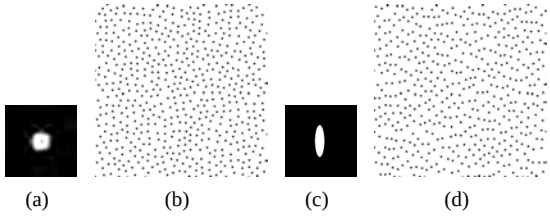

Figure 10: *Distributed points using Poisson-disk distribution. (a) (c) Shape of Disk for distribution. White region indicates exclusive region. (b) (d) Distributed points using (a) and (c).*

6. Conclusion and Future work

In this paper, we proposed a simple generation method for realistic cattle leather texture by placing structural elements. We observed noticeable structures on real leather and classified them into five elements, which are crista, sulcus, wrinkle, pocket and pore. To place skeletons of elements, our method first places cristae, sulci and pockets based on anisotropic Voronoi diagram, then adds new lines for the wrinkles and new points for the pores. Finally the method calculates three-dimensional shape with radial based functions according to the distance from placed elements.
The proposed method generates detailed leather texture including most noticeable structural elements that previous methods [MHZ94, WKMT99, IMS03, MSI*06, SMKM07]

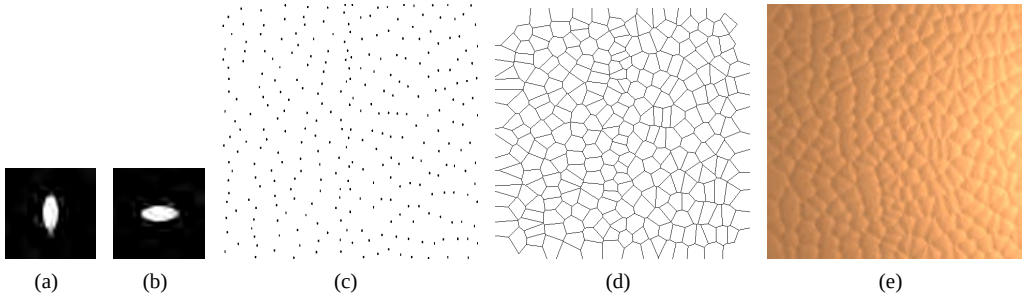

Figure 11: *Distribution result (a)(b) Exclusive regions. (c) Distributed sites using (a) for left side and (b) for right side. (d) Voronoi diagram from (c). (e) Leather texture generated from (d).*

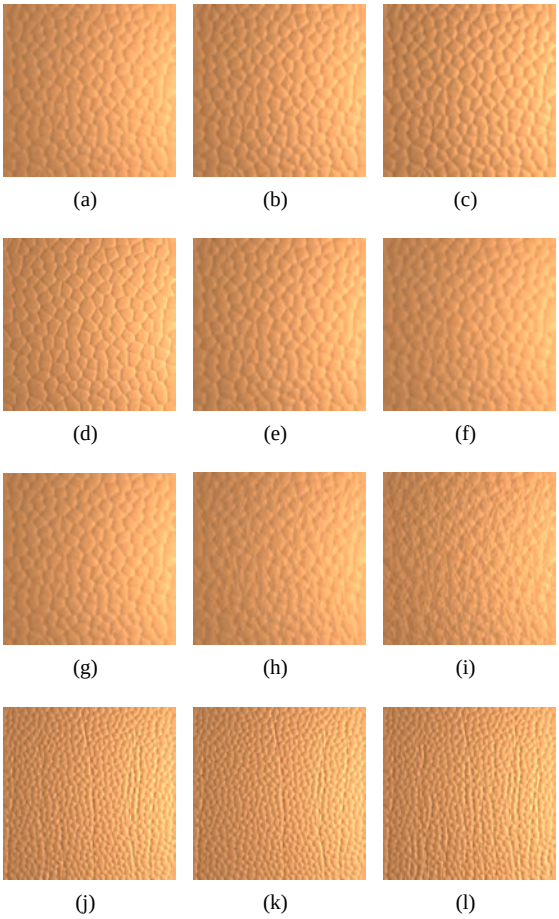

Figure 12: *Changes of generated texture. These parameters are described in Table 1.*

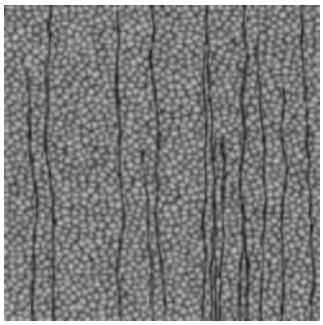

Figure 13: *Generated texture from Fig. 1(a)*

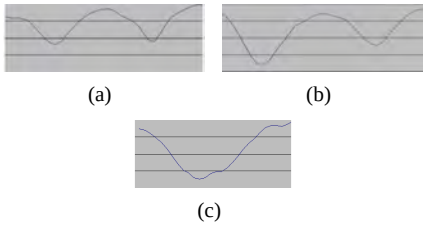

Figure 14: *Cross-sections of a portion of generated texture from Fig. 13. (a) sulcus (b) wrinkle and sulcus. (c) pocket*

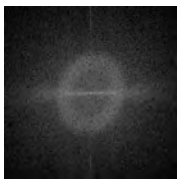

Figure 15: *Power spectral density of generated texture from Fig. 13*

do not include and is easy to handle with its simple procedures and intuitive parameters.
A limitation of our method is that it only generates a cattle leather texture by the construction from the five elements. Also the method has a possibility to generate other animal leathers which possess same or less structures and elements with cattle leather such as sheep. The method does not generate other elements or structures, for example ostrich leather that includes circular protuberances called crowns. It is required to redefine concerning additional elements or different structures for generating wider range of animal leather.

References

[CGS06] CHEN T., GOESELE M., SEIDEL H.-P.: Mesostructure from specularity. *CVPR '06: Proc. The 2006 IEEE Computer Society Conference on Computer Vision and Pattern Recognition 2* (2006).

[DB97] DE-BONET J.: Multiresolution sampling procedure for analysis and synthesis of texture images. *Proc. of ACM SIGGRAPH 97* (1997), 361–368.

[DEJ*99] DORSEY J., EDELMAN A., JENSEN H. W., LEGAKIS J., PEDERSEN H. K.: Modeling and rendering of weathered stone. *Proc. of ACM SIGGRAPH 99* (1999), 225–234.

[EL99] EFROS A., LEUNG T.: Texture synthesis by non-parametric sampling. *International Conference Computer Vision* (1999).

[HB95] HEEGER D. J., BERGEN J. R.: Pyramid-based texture analysis/synthesis. *Proc. of ACM SIGGRAPH 95* (1995), 229–238.

[HEG01] HARO A., ESSA I. A., GUENTER B. K.: Real-time photo-realistic physically based rendering of fine scale human skin structure. *Proc. of The 12th Eurographics Workshop on Rendering Techniques* (2001).

[IMS03] ITOH T., MIYATA K., SHIMADA K.: Generation of organic textures with controlled anisotropy and directionality via packing rectangular and elliptical cells. *IEEE CG &A 23 3* (2003), 38–46.

[IYYT93] ISHII T., YASUDA T., YOKOI S., TORIWAKI J.: A generation model for human skin texture. *Proc. of CGI 93* (1993), 139–150.

[MHZ94] MCCARTNEY J., HINDS B. K., ZHANG J. J.: Leather texture synthesis and rendering. *Computer & Graphics 18* (1994), 87–92.

[Miy90] MIYATA K.: A method of generating stone wall patterns. *Proc. of ACM SIGGRAPH 90 24 4* (1990), 387–394.

[MSI*06] MIYATA K., SAKAGUCHI Y., IMAO K., HATADA Y., FUJITA A., SUZAKI R.: Leather texture generation. *ACM SIGGRAPH 2006 Research Poster* (2006).

[PH89] PERLIN K., HOFFERT E.: Hypertexture. *Proc. of SIGGRAPH 89* (1989), 253–262.

[PPWE02] PEACHEY F. K. M. . D., PERLIN K., WORLEY S., EBERT D. S.: *Texturing and Modeling: A Procedural Approach (Morgan Kaufmann Series in Computer Graphics and Geometric Modeling)*. Morgan Kaufmann, 2002.

[SMKM07] SAKURAI K., MIYATA K., KAWAI N., MATSUFUJI K.: Leather texture generation considering sulci flow. *Proc. of IEVC2007 1B-1* (2007), 1–6.

[SP98] SIMONCELLI E., PORTILLA J.: Texture characterization via joint statistics of wavelet coefficient magnitudes. *Proc. of Fifth International Conference on Image 1* (1998), 62–66.

[Tur91] TURK G.: Generating textures for arbitrary surfaces using reaction-diffusion. *Proc. of ACM SIGGRAPH '91 Computer Graphics 25 No. 4* (1991), 289–298.

[Wen95] WENDLAND H.: Piecewise polynomial positive definite and compactly supported radial basis functions of minimal degree. *Advances in Computational Mathematics 4* (1995), 389–396.

[WK91] WITKIN A., KASS M.: Reaction-diffusion textures. *Proc. of ACM SIGGRAPH 91 Computer Graphics 25 No. 4* (1991), 299–308.

[WKMT99] WU Y., KALRA P., MOCCOZET L., THALMANN N. M.: Simulating wrinkles and skin aging. *The Visual Computer 15 4* (1999), 183–198.

[WKT96] WU Y., KALRA P., THALMANN N. M.: Simulation of static and dynamic wrinkles of skin. *Proc. of The Computer Animation* (1996), 90–97.

[WKT97] WU Y., KALRA P., THALMANN N. M.: Physically-based wrinkle simulation and skin rendering. *Proc. of Eurographics Workshop on Computer Animation and Simulation 97* (1997), 69–79.

[WL00] WEI L. Y., LEVOY M.: Fast texture synthesis using tree-structured vector quantization. *Proc. of ACM SIGGRAPH 2000* (2000), 479–488.

[Wor96] WORLEY S.: A cellular texture basis function. *Proc. of SIGGRAPH 96* (1996).

[ZWM98] ZHU S., WU Y., MUMFORD D.: Filters, random fields and maximum entropy towards a unified theory for texture modeling. *International Journal of Computer Vision 27 2* (1998), 107–126.

[ZZV*03] ZHANG J., ZHOU K., VELHO L., GUO B., SHUM H.-Y.: Synthesis of progressively-variant textures on arbitrary surfaces. *Proc. of ACM SIGGRAPH 2003* (2003), 295–302.

Table 1: *Parameters. Generation size is 500 × 500 pixels. Parameters are crista height h_c, sulcus height h_s, sulcus width w_s, bold height h_b, bold width w_b, pocket height h_p, pocket width w_p, pore height h_q, pore width w_q, crista shape coefficient n, invasion parameter l, length of wrinkle b_l, angle of bold b_a, vector of bold $\boldsymbol{b}$, number of bolds bn*

	h_c	h_s	w_s	h_b	w_b	h_p	w_p	h_q	w_q	n	l	b_l	b_a	$\boldsymbol{b}$	bn
Fig. 12 (a), (e) and (g)	255	80	20	-	-	80	10	20	5	2	0	-	-	-	-
Fig. 12 (b)	255	85	20	-	-	80	10	20	5	2	0	-	-	-	-
Fig. 12 (c)	255	113	20	-	-	80	10	20	5	2	0	-	-	-	-
Fig. 12 (d)	255	80	10	-	-	80	10	20	5	2	0	-	-	-	-
Fig. 12 (f)	255	80	30	-	-	80	10	20	5	2	0	-	-	-	-
Fig. 12 (h)	255	80	20	-	-	80	10	20	5	2	10	-	-	(0,1)	-
Fig. 12 (i)	255	80	20	-	-	80	10	20	5	2	20	-	-	(0,1)	-
Fig. 12 (j)	255	80	20	60	25	80	10	20	5	2	0	500	30	(0,1)	5
Fig. 12 (k)	255	80	20	60	25	80	10	20	5	2	0	500	30	(0,1)	10
Fig. 12 (l)	255	80	20	60	25	80	10	20	5	2	0	500	30	(0,1)	30

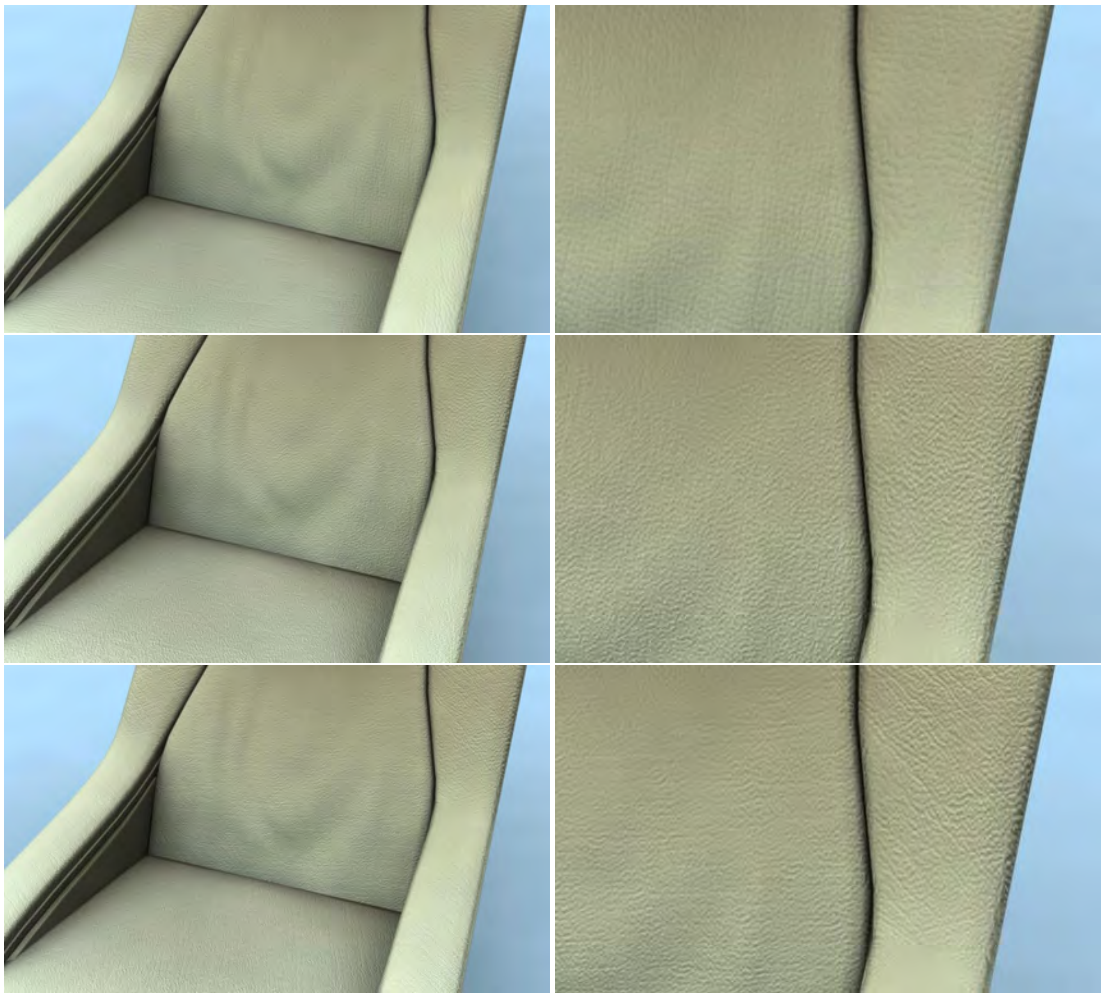

Figure 16: *Bump mapping with generated leather texture*